D" reflection polarities inform lowermost mantle mineralogy

Christine Thomas[1,1], Laura Cobden[2,2], and Art R. T. Jonkers[1,1]

[1]University of Muenster
[2]Utrecht University

November 30, 2022

Abstract

Polarities of seismic reflections at the discontinuity atop the D" region (PdP and SdS) indicate the sign of the velocity contrast across the D" reflector. Recent studies found PdP polarities matching and opposite those of P and PcP. While anisotropy could explain this behavior, we find that the ratio of the change in S-wave velocity over change in P-wave velocity (R-value) can influence polarity behavior of D" reflected P-waves. For R-values exceeding 3 the P-wave reverses polarity in the absence of anisotropy while S-wave polarity is not influenced by the R-value. Using sets of 1 million models for normal mantle and MORB with varying minerals and processes across the boundary, we carry out a statistical analysis (Linear Discriminant Analysis) finding that there is a marked difference in mantle mineralogy to explain R values larger and smaller than 3, respectively. Based on our results we can attribute different mineralogy to a number of cases. In particular, we find that when velocities increase across D" and polarities of PdP and SdS are opposite the post-perovskite phase transition is still the best explanation while MORB is the best explanation when PdP and SdS are the same. When the velocities are decreasing, the post-perovskite phase transition within MORB is the best explanation if PdP and SdS polarities are the same but if PdP and SdS are opposite in regions of velocity decreases, our results indicate that primordial material or mantle enriched in bridgmanite can explain the polarity behavior, further constraining mineralogy within the LLSVPs.

Hosted file

`thomas_suppinfo_revised.docx` available at https://authorea.com/users/559933/articles/608238-d-reflection-polarities-inform-lowermost-mantle-mineralogy

D" reflection polarities inform lowermost mantle mineralogy

C. Thomas[1], L.J. Cobden[2], A.R.T. Jonkers[1]

1 Institut für Geophysik, Westfälische Wilhelms-Universität Münster, Correnstr 24, 48149 Münster, Germany

2 Department of Earth Sciences, Princetonlaan 8a, Universiteit Utrecht, 3584CB Utrecht, The Netherlands

Corresponding author: Christine Thomas (cthom_01@uni-muenster.de)

Key Points:

- Ratio (R) of S- over P-wave velocity changes (%) controls polarity of P-wave reflections at D" reflector.
- Thermochemical modelling and statistical analysis show specific minerals contributing to large R values.
- Polarity observations indicate that part of the Pacific LLSVP is due to bridgmanite enrichment.

Abstract

Polarities of seismic reflections at the discontinuity atop the D" region (PdP and SdS) indicate the sign of the velocity contrast across the D" reflector. Recent studies found PdP polarities matching and opposite those of P and PcP. While anisotropy could explain this behavior, we find that the ratio of the change in S-wave velocity over change in P-wave velocity (R-value) can influence polarity behavior of D" reflected P-waves. For R-values exceeding 3 the P-wave reverses polarity in the absence of anisotropy while S-wave polarity is not influenced by the R-value. Using sets of 1 million models for normal mantle and MORB with varying minerals and processes across the boundary, we carry out a statistical analysis (Linear Discriminant Analysis) finding that there is a marked difference in mantle mineralogy to explain R values larger and smaller than 3, respectively. Based on our results we can attribute different mineralogy to a number of cases. In particular, we find that when velocities increase across D" and polarities of PdP and SdS are opposite the post-perovskite phase transition is still the best explanation whereas MORB is the best explanation when PdP and SdS are the same. When the velocities are decreasing, the post-perovskite phase transition within MORB is the best explanation if PdP and SdS polarities are the same but if PdP and SdS are opposite, our results indicate that primordial material or mantle enriched in bridgmanite can explain the polarity behavior, further constraining mineralogy within the LLSVPs.

Plain Language Summary

The polarities of seismic waves (P and S) reflecting at structures in the Earth´s mantle indicate seismic velocity changes across those structures. For the lowermost mantle reflector (called D" reflector, approx. 300 km above the core-mantle boundary), a velocity increase for P- and S-waves across the boundary generates a polarity that is the same for the main wave and the core-reflected wave. If, however, the percentage change of the velocity of the S-wave increases at least three times as much as that of the P-wave velocity (expressed as the R-value, the ratio dVs/dVp), the polarity of the D"-reflected PdP wave changes polarity, becoming opposite to both the main P-wave and the reflection from the core-mantle boundary below it. Here we analyse sets of one million models with variable compositions of mantle material and mid-ocean ridge basalt and use an advanced statistical method to identify those combinations of minerals that produce large positive R-values. Two scenarios are distinguished: P- and S-velocity both increasing, and both decreasing. In each of these, the reflected P-wave polarity can be either the same as, or opposite to, the S-wave polarity, yielding four cases in total. We find that previous explanations for three of these cases concur with our analysis. However, for regions where velocities decrease over the D" reflector but polarities of P and S-wave reflections are opposite, our analysis shows that enrichment with the lower-mantle mineral bridgmanite is mainly responsible for the observed polarity behaviour. This suggests that for regions such as large low-velocity anomalies in the lowermost mantle, primitive or bridgmanite-enriched material is the preferred explanation. More generally, this study shows that waveforms and polarities of seismic waves are useful in constraining lowermost mantle mineralogy.

1 Introduction

The lowermost mantle of the Earth, the D" region (Bullen, 1949), is characterised by a range of seismic structures that have been studied with a variety of seismic methods, in order to understand their formative processes and mineralogy in the deep Earth (for overviews, see Garnero, 2000; Lay, 2015). One prominent feature of the lowermost mantle is a seismic discontinuity at the top of the D" region that generates reflections for S- and P-waves (see reviews by Wysession et al., 1998; Lay, 2015; Cobden et al., 2015; Jackson and Thomas, 2021). Several explanations for this reflector at the top of D" have been discussed, such as subducted slabs (e.g., Lay and Garnero, 2004), scatterers (Scherbaum et al., 1997), and the post-perovskite phase transition (e.g., Murakami et al., 2004; Oganov and Ono, 2004; Tsuchiya et al., 2004; Shim, 2008).

The D" reflector has been found in many regions at approximately 300 km above the CMB, constrained mostly by travel times of the reflected waves off the top of D" (Lay and Helmberger, 1983; Weber, 1993; Wysession et al., 1998; Cobden et al., 2015) with depth variations of about ± 100 km. But whereas in the past travel times of seismic data were most commonly used for studying the reflector, recently wave amplitudes and polarities have also been used to extract details about D" structures (e.g., Cobden and Thomas, 2013; Thomas et al., 2011; Thorne et al., 2007; Pisconti et al., 2019). For example, complexity in waveforms can indicate layering (e.g. Moore et al., 2004; Thomas et al., 1998; Rost et al., 2005; Schumacher et al., 2018), and wave amplitude behaviour has provided information on attenuation (e.g., Lay and Helmberger, 1981; Cormier, 1982) or gradients of seismic reflectors in the Earth (e.g., Lay, 2008; Weber 1993). In addition, polarities of seismic waves can provide information about velocity and density variations, i.e., the impedance contrast, across a reflector (Zoeppritz, 1919).

Previous work on D" reflections (e.g., Weber, 1993; Lay and Helmberger, 1983; Cobden et al., 2015; Cobden and Thomas 2013) has shown that the polarities of these reflected P- or S-waves correlate with the velocity jump across the reflector. This means that for a P-wave velocity increase across D", the reflection off this layer (PdP, see Figure 1a) will show the same polarity as both the direct P-wave travelling above it and PcP, the P-wave reflection off the core-mantle boundary. The same is true for S-waves. Lay et al. (2004) stated that the density has little influence on amplitudes of the reflected waves at epicentral distances exceeding 60 degrees, therefore models have often been calculated based only on the change in Vp and Vs (e.g., Lay and Helmberger, 1983; Young and Lay, 1990; Weber, 1993). The magnitude of the velocity jump is generally determined by comparing the observed amplitude of the reflected wave with synthetic predictions, often using 1D modelling (e.g. Weber 1993; Lay and Helmberger, 1983). The estimated wave-velocity jumps usually range from 1-3%, but can occasionally reach 5% (Bréger and Romanowicz, 1998; Thomas and Laske, 2015).

Interestingly, recent observations of PdP-wave polarities have in some cases shown opposite polarities to PcP- and P waves (e.g., Thomas et al., 2011; Hutko et al., 2008; Pisconti et al., 2019), which would suggest a seismic velocity reduction across the reflector, while SdS waves in these regions show polarities that agree with S and ScS, indicating a positive velocity jump across D" (e.g., Chaloner et al., 2009; Cobden and Thomas, 2013; Thomas and Laske, 2015). This discrepancy between PdP and SdS polarities excludes a purely thermal origin, since one would expect both velocities to increase given a temperature reduction. The mineral phase transition of bridgmanite to post-perovskite in MgSiO3 (Murakami et al., 2004; Oganov and Ono, 2004; Shim et al., 2004; Tsuchiya et al. 2004), which occurs near the core-mantle boundary (CMB), has been shown in theoretical mineral physics calculations to be potentially associated with a small change in P wave-velocity (which can be either positive or negative) and a larger increase (of up to 3%) in S wave-velocities (Wookey et al., 2005; Tsuchiya and Tsuchiya, 2006; Wentzcovitch et al., 2006; for a compilation of published wave velocity changes in D" related to the post-perovskite phase transition, see Cobden et al., 2015). Hence the presence of post-perovskite could potentially explain these discrepant PdP- and SdS polarity observations. In other regions, however, the PdP wave exhibits the same polarity as P and PcP, while SdS also shows the same polarity as S and ScS (Weber, 1993; Thomas et al., 1997; Cobden and Thomas 2013). This would make pure MgSiO3 post-perovskite (Wookey et al., 2005) an unlikely explanation for the D" reflector in those places (e.g., Cobden and Thomas, 2013), but the latter could still be caused by post-perovskite if the P-wave velocity change is positive across the phase transition (e.g., Tsuchiya and Tsuchiya, 2006).

It has been shown (Thomas et al., 2011; Pisconti et al. 2019) that in some areas P-wave polarity depends on the direction of wave propagation (i.e., azimuth) and that deformation, i.e., anisotropy in D", can change the polarity of P-waves and potentially also S-waves (Thomas et al., 2011; Creasy et al., 2019; Pisconti et al., 2019). To our knowledge, array observations of SdS waves with an opposite polarity to S and ScS have not been reported, but stacks of seismic data (e.g., Lay et al., 2006) and inversions (Kawai and Geller, 2010; Konishi et al., 2009) suggest that velocity decreases for S-waves also exist. Using azimuthal as well as distance dependence of the polarities of P- and S-wave D" reflections can help to further constrain mineralogy in D" (Creasy, et al., 2019; Pisconti et al., 2019, 2022).

Most aforementioned observations have been made in regions where tomographic inversions suggest above-average velocities (Ritsema et al., 2011; Hosseini et al., 2018, 2020; Li et al., 2008). If deep subduction is responsible for the D" reflector in these cases, a post-perovskite phase transition would be a good explanation, since post-perovskite would preferably be found in colder mantle regions (e.g. Hernlund et al., 2005; Cobden and Thomas, 2013; Cobden et al., 2015). Moreover, this would also agree with the mineralogical best fit for anisotropy in post-perovskite (Pisconti et al., 2019; Creasy et al., 2019; Romanowicz and Wenk, 2017; Thomas et al., 2011).

For regions associated with below-average wave speeds, it has been suggested that observations of PdP and SdS reflections may not be due to a simple Mg-bridgmanite to post-perovskite phase transition, due to the positive Clapeyron slope of the phase transition (Murakami et al., 2004; Oganov and Ono, 2004), and the possibility that slower-than-average regions may be warmer (e.g. Hernlund et al., 2005). However, when this phase transition takes place in Fe- and Al-bearing bridgmanite, or in a multi-mineral assemblage, then the depth and strength of the discontinuity can change, as well as introducing a broad depth interval over which the transition occurs (e.g. Grocholski et al., 2012, Catalli et al., 2009, Cobden et al., 2015, Hernlund, 2010, Kuwayama et al., 2022), even moving the phase transition to pressures inside the core. A broad phase transition region may make observations of the seismic reflector off this phase transition more difficult to observe since it results in small amplitudes of D" reflected waves. Interestingly, in some of these low-velocity regions, P (and S, respectively) wave reflections off D" show the same polarity as the direct P-wave (S) and core reflected PcP wave (ScS). This indicates an increase in seismic wave velocity across D", even though a tomographic model might suggest slow wave velocities regionally, which would lead to an opposite polarity for a reflection from these regions (e.g. Jackson and Thomas, 2021, Cobden et al., 2013). However, one should be cautious when comparing D" reflection points with tomographic models in detail, since the latter is concerned with large-scale lateral variations in wave velocity, and a lack of model resolution and other uncertainties limit the interpretation of structures at the relatively small length scale of D" reflection points. Also, lateral homogeneity in a tomography model does not preclude vertical changes in wave velocity.

In summary, polarity observations of P and S-waves reflecting off the D" region seem variable, and while anisotropy could potentially explain these variations, here we investigate whether an alternative explanation could also produce polarity changes of D" reflections.

2 Modelling of polarities

The reflection coefficient is controlled by the impedance contrast (density × velocity) for P- and S waves across a discontinuity, and the angle of incidence of the wave at the discontinuity (Zoeppritz, 1919, see also descriptions and approximations in Aki and Richards, 1980; Bortfeld, 1961). The amplitudes of reflected and transmitted waves for an incoming P- or S-wave are governed by the velocities of P- and S-waves, by density (impedance) contrasts and also ratios of P- and S-wave velocities above and below the boundary. For a reflection off the top of the discontinuity, the reflection coefficient will, for sufficiently large angles of incidence, enter the overcritical range (e.g., Weber, 1993), causing a phase change and strongly enhancing the amplitude of the reflection (see Figure 1b-d). For this reason, most previous D" reflection studies favour a distance range of 65 to 85 degrees (e.g., Wysession et al., 1998; Lay, 2015; Cobden et al., 2015 for reviews) to benefit from large amplitudes.

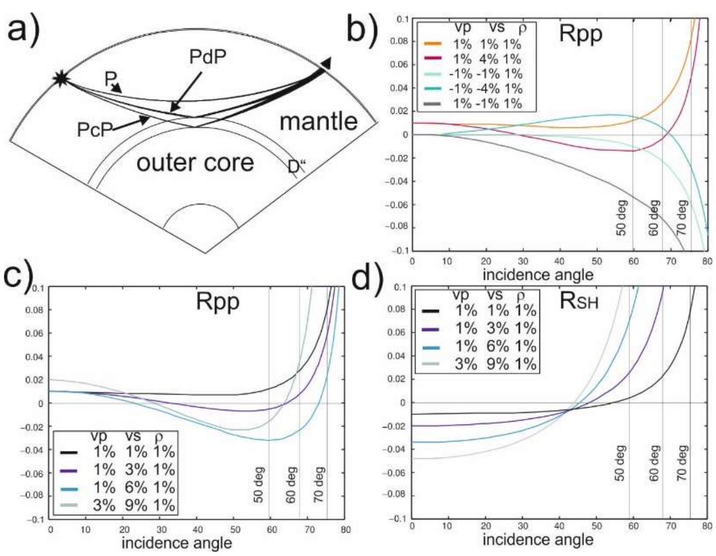

Figure 1: a) wave paths of P waves, the reflection off the D" discontinuity PdP, and PcP, the CMB-reflected phase. Same paths for S, SdS and ScS. b) Reflection coefficient for P to P reflections (Rpp) at the D" discontinuity with variable changes in Vp, Vs and density across the reflector as given in the legend. c) Same as for b but for different (but only positive) values of the

changes in Vp and Vs across D". d) Same as c) but for SH to SH reflection coefficient (RSH). The distance corresponding to the incidence angle at the discontinuity is given by the vertical lines in b, c, and d.

To investigate polarities of D" reflections (PdP and SdS, Figure 1a), we vary P-and S-wave velocity jumps (d*Vp* and d*Vs*) as well as the density jump across the boundary, compute the reflection coefficient for P and SH wave reflections. We verify the results using three different methods (Reflectivity method, Müller, 1985; Zoeppritz explorer (Crewes Explorer programs 2022) and Javascript solver for Zoeppritz equations (Frederiksen 2022). For completeness we also tested converted waves (PdS and SdP waves) and SV reflections, although those have not been used extensively for D" studies. We express the velocity changes of *Vp* and *Vs* through the (R)atio of percent *Vs* change over percent *Vp* change, the so-called R-value (similar to the concept of R in seismic tomography, e.g., Masters et al., 2000; Karato and Karki, 2001; Koelemeijer et al., 2016). Thus a 1% change in *Vp* in combination with a 3% change in *Vs* would yield an R-value of 3.

We confirm that for the distance ranges often used for D" reflection observations (65-85 degrees distance), which correspond to incidence angles above 70 degrees (Figure 1b-d), a velocity increase in *Vp* produces the same polarity as that of P and PcP (and ditto for S-waves). However, we find that from an R-value of 3, which means that the %-change of *Vs* is at least 3 times that of the %-change of *Vp*, the reflection coefficient for the P-wave becomes negative for part of the incidence angle range (Figure 1b and 1c). The size of the reflection coefficient increases with increasing P-wave velocity jump (blue and grey lines compared with black line in Fig 1c), but the R-value determines whether for part of the incidence angle range the P-wave reflection coefficient becomes smaller than zero, resulting in a PdP wave polarity opposite to that of P and PcP (black line versus blue and grey lines in Figure 1c). The same is true for P-wave reflection coefficients for negative *Vp* and negative *Vs* changes (Figure 1b).

However, if either *Vp* or *Vs* increases while the other velocity decreases, this effect does not occur. Taking the case of a small P-wave velocity reduction with an S-wave velocity increase (negative R-value, dark grey line in Figure 1b), as is expected for the bridgmanite to post-perovskite phase transition in MgSiO3 (e.g., Wookey et al., 2005), this yields a PdP-wave polarity opposite to that of P waves, as expected for velocity reductions, but no polarity change over the entire incidence angle range occurs for all R-values. But such a case of opposite changes for P- and S-wave contrasts causes amplitudes to be slightly larger than for changes with the same signs (see also Cobden et al., 2015).

Due to the reflection coefficient becoming negative for part of the incidence angle range, as shown in Figure 1b-d, the reflection coefficient also has up to two angles (Brewster angles, in analogy to optics, Yang et al., 2021; Tatham and Kreil, 2012; Červený, 2001) where no P-wave is reflected in case of an incident P-wave. The same is true for an incident S-wave, however, only one Brewster angle is usually found there (e.g., Müller, 2007, Červený, 2001). Waves do behave non-intuitively at interfaces (see also Malcolm and Trampert 2011; Sollberger et al., 2017), so it is not straightforward to explain the physical reason behind the behaviour of reflection coefficients, but it is likely that it arises due to the interaction (and production) of the

SV wave at the interface, as well as the reflected and transmitted P-wave, together with the relevant boundary conditions (Červený, 2001).

Looking at the SH-wave reflection coefficient, we find that an R-value smaller or larger than 3 does not affect the polarity of the S-wave reflection much in the distance range used for observing D" reflections; it mostly changes the amplitude of the wave (Figure 1d) and, to a small degree, the incidence angle at which the polarity change occurs, which always happens for the S-wave reflection coefficient (e.g., Müller, 2007). The S-wave reflection coefficient shows a polarity change for incidence angles smaller than 50 degrees, which translates into small epicentral distances (< 40 to 45 degrees, depending on P and S-velocity changes, see Figure 1d), so usually it is not tested for D" studies. For the larger epicentral distances often used in D" studies (i.e. 65 degrees and above), the SdS-wave will therefore always show a polarity that is the same as the S-wave for velocity increases. We also found that that PdS and SdP waves and vertically polarised SdS waves show no change in polarity with varying R-values, only a change in the size of the reflection coefficient, leading to amplitude changes of the waves. Thus, we concentrate in the following on the polarity behaviour of PdP waves only.

So far, we have only looked at changes in *Vp* and *Vs*. Lay et al. (2004) mention that the density has little effect on the amplitude of the reflected wave and therefore on the reflection coefficient for epicentral distances of 70 degrees and larger, and in our studies this is indeed the case, even for large R-values. Regarding smaller distances, the change in density does not influence the incidence angle at which the reflection coefficient changes polarity, but it does affect the amplitude of the wave at short incidence angles, i.e., at distances below 10-20 degrees.

For R-values of 3 and 4, the epicentral distance that corresponds to the incidence angle at which the PdP wave reverses polarity is smaller than that used in most studies, and only short-distance data of 40 to 65 degrees would allow detection of this reflection coefficient polarity behaviour (Figure 1b). Few observed steep-angle D" reflections have been reported so far (e.g., Schimmel and Paulssen, 1996 (using S-waves), Thomas and Laske, 2015 (using P-waves)), mostly because the amplitudes are so small that the reflections have to be detected using stacking methods (e.g., Weber 1993; Thomas et al., 2004a,b; Kito et al., 2007; Cobden and Thomas 2013). Increasing the size of the R-value shifts the transition from a negative to a positive reflection coefficient (i.e., from opposite to same polarity of PdP with respect to P) to larger epicentral distances, allowing this behaviour to also be observed at larger distances; however, very large R-values (R > 5) may be unrealistic for the Earth.

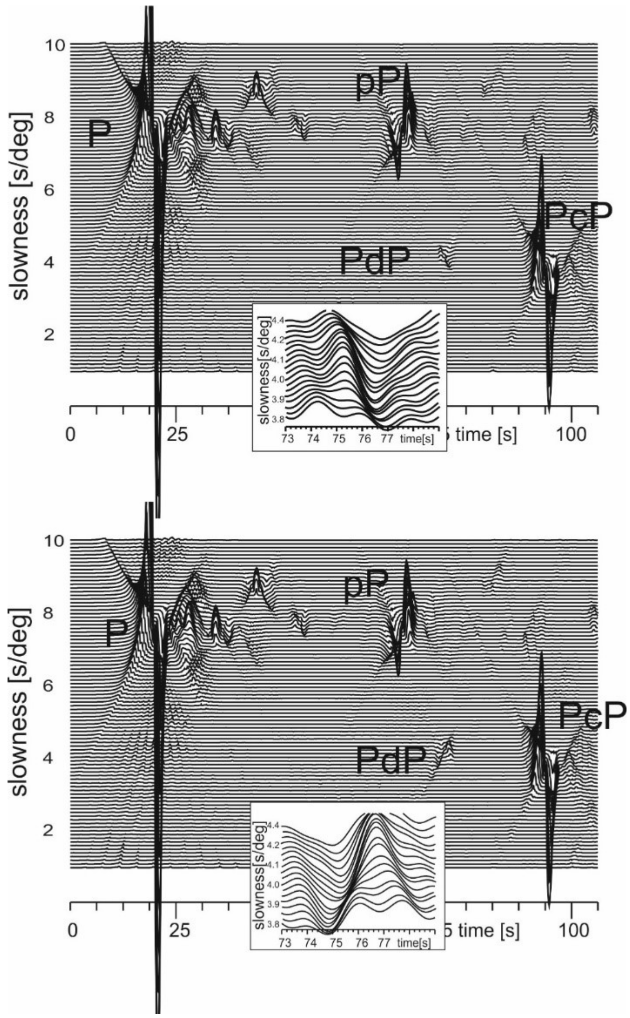

Figure 2: 4th root vespagrams for two synthetic data examples: top: an R-value of 2, bottom: an R-value of 6. The insets show the PdP wave for a better comparison with P and PcP waveforms and polarities. The arrival at 75 sec with P-slowness is the pP wave.

The behaviour of the reflection coefficient allows us to test the ratio of changes in P-velocity versus S-velocity, which may help to constrain the mineralogy of the D" region and the cause for the observed D" reflector. But because the reflection coefficient is very small, it is necessary to test whether a D" reflection would still be visible in seismic data. To confirm our reflection coefficient findings, we use the reflectivity method (Müller, 1985) to generate synthetic data for R-values larger and smaller than 3. Since PdP arrivals are usually small in a seismogram, we generate 4th root vespagrams (e.g., Davies et al., 1971; Muirhead and Datt, 1976; Rost and Thomas, 2002; Schweitzer et al., 2002) in which these arrivals can be detected and distinguished by their slowness values. Vespagram processing has been used in many studies to detect P- and S-wave reflections off the D" discontinuity (e.g., Weber, 1993; Thomas and Weber, 1997; Kito et al., 2007; Thomas et al., 2004a,b; Cobden and Thomas, 2013, Pisconti et al., 2019). Figure 2a shows an example vespagram for synthetic data generated by a model with a velocity increase across D" and an R-value of 2. Contrastingly, Figure 2b shows a vespagram for a model with a velocity increase across D" and an R-value of 6. The inset shows the PdP wave; one can clearly see that the polarity of PdP of Figure 2b is opposite to that of P and PcP, while in Figure 2a the PdP polarity is the same as that of P and PcP. The vespagrams are generated for stations in an epicentral distance of 45 to 52 deg. To demonstrate that the change in polarity is distance-dependent, Figure 3 shows the traces for 62 and 48 degrees for the case of an R-value of 1 (black curve) and an R-value of 4 (red curve). The wave at 48 degrees arriving at 52 s is the depth phase pP, which can be distinguished by its slowness in the vespagram in Figure 2.

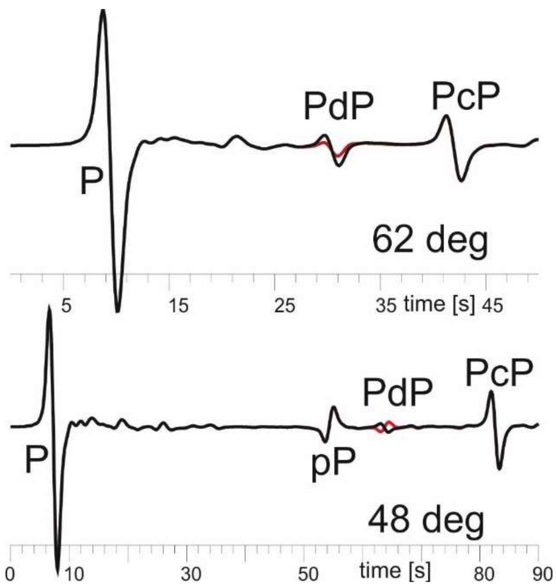

Figure 3: Seismogram section for the model with R-value of 2 (black line) and R-value of 6 (red line) for two different distances, indicating the distance dependency of the polarity reversal. The P and PcP waves are clearly visible in both examples, the arrival at 52 sec in the seismogram for 48 deg is the pP wave.

3 Comparison with Data

Our modelling shows that an observation of the effect of R-values larger than 3 on seismic polarities is theoretically possible. We searched the literature for evidence of published R-values greater than 3 in the lower mantle, but found most published velocity ratios for the D" region in the range of 1 to 3, where a ratio of 3 is often interpreted as melt (Williams and Garnero, 1996; Jackson and Thomas, 2021; Dobrosavljevic et al., 2019, Rost et al., 2005). Tomographic inversions show R-values ($\mathrm{dln}Vs/\mathrm{dln}Vp$ in this case) of up to 5 in the lowermost mantle (Koelemeijer et al., 2016, 2018) and even higher (Cobden et al., 2012). Mineralogically, R-values larger than 3 are possible (Deschamps & Trampert, 2003; Hernlund & Houser 2008; Cobden et al., 2012; Karato and Karki, 2001) and should generate polarity reversals for part of the distance range. In fact, high P-T experiments suggest that for Fe-rich (Mg,Fe)O, the R-value could be up to 6-9 if Reuss-bound mixing models are employed (e.g., Dobrosavljevic et al., 2019). It is therefore necessary to assess the polarity of PdP waves at short distances in real data, to verify our modelling results.

Most PdP wave reflections have been detected for large epicentral distances (larger 60 degrees) and cases of opposite as well as the same PdP polarity compared with the main phases (PcP and P) have been found. In contrast, most SdS reflections seem to have the same polarity as ScS and S, except for the Pacific (Lay et al., 2006; Ohta et al., 2008). An overview of previously observed polarities for PdP waves can be found in Cobden and Thomas (2013) or Cobden et al. (2015). A recent study (Pisconti et al., 2019) detected PdP and SdS waves beneath the Central Atlantic near the edge of the large velocity anomaly beneath Africa. In their work, the PdP waves for shorter distances showed opposite polarities with respect to P, while the SdS-waves had the same polarity as S for all distances. This polarity behaviour is possible for an R-value exceeding 3, but is more likely for an R-value of about 5, since the angle of incidence at which the polarity changes sign (Fig. 1) occurs at larger epicentral distances for R =5 than for R=3. Pisconti et al. (2019) showed that deformation of post-perovskite, i.e., anisotropy, could be responsible for those variations in polarity of PdP, especially since they also used splitting measurements for the same region. It would be of interest to investigate a crossing path for this particular region to test their interpretation of anisotropy versus the possibility of large R-values.

To examine other locations, we collected data from a number of seismic arrays to find D" reflections at short distances (between 40 and 60 degrees) where we would expect a change in polarity of PdP if the R-value is larger than 3. Despite a large number of source-receiver combinations, we found only a small number of events that show an additional arrival in vespagram analysis (e.g., Rost and Thomas, 2002; Schweitzer et al., 2002) with a slowness and travel time that agree with a D" reflection. Since reflection coefficients for the selected distance range of 40-60 degrees are small (Figures 1), the reflection is often very small in the vespagram or might be buried in noise. Nevertheless, we were able to find a few cases where the polarity of the D" reflection can be extracted and compared with PcP and P (Figure 4). We verify that the D" reflections travel in plane by performing slowness-backazimuth analyses, as shown for one example event in Figure S1. It is possible that reflections that travel out-of-plane could arrive with an opposite polarity due to the radiation pattern or reflections at different structures, i.e., not D" (Schumacher and Thomas, 2016; Schumacher et al., 2018, Rochira et al., 2022), therefore, in our study, we ensure that all waves travel in plane.

Two examples of D" reflections shown are from events in the Mariana region, detected at an array in Tibet (Tables S1 and S2), for which the distances are 49 and 51 degrees. One of these D" reflections, located beneath the western Pacific, shows a polarity that is the same as PcP and P (Figure 4a, d), while the other shows an opposite polarity (Figure 4b, e). The region in D" where these two events reflect is associated with high to average P-wave velocities in most tomographic models (e.g. Hosseini et al., 2020; Simmons et al., 2010), or a change from high- to low velocity as shown in Figure 4g for the tomographic model of Li et al. (2008). The third data example in Figure 4 is an event in Chile recorded at the Transportable Array (TA) stations in Kentucky (Tables S1 and S2), with an epicentral distance of 62 degrees. The vespagram of this event shows a reflection with the same polarity as P and PcP (Figure 4c, f). This event is reflecting in an area characterised by past subduction (Figure 4h), and tomographic inversions for P-waves show mostly fast velocities here (e.g. Hosseini et al., 2020; Li et al., 2008; Simmons et al., 2010).

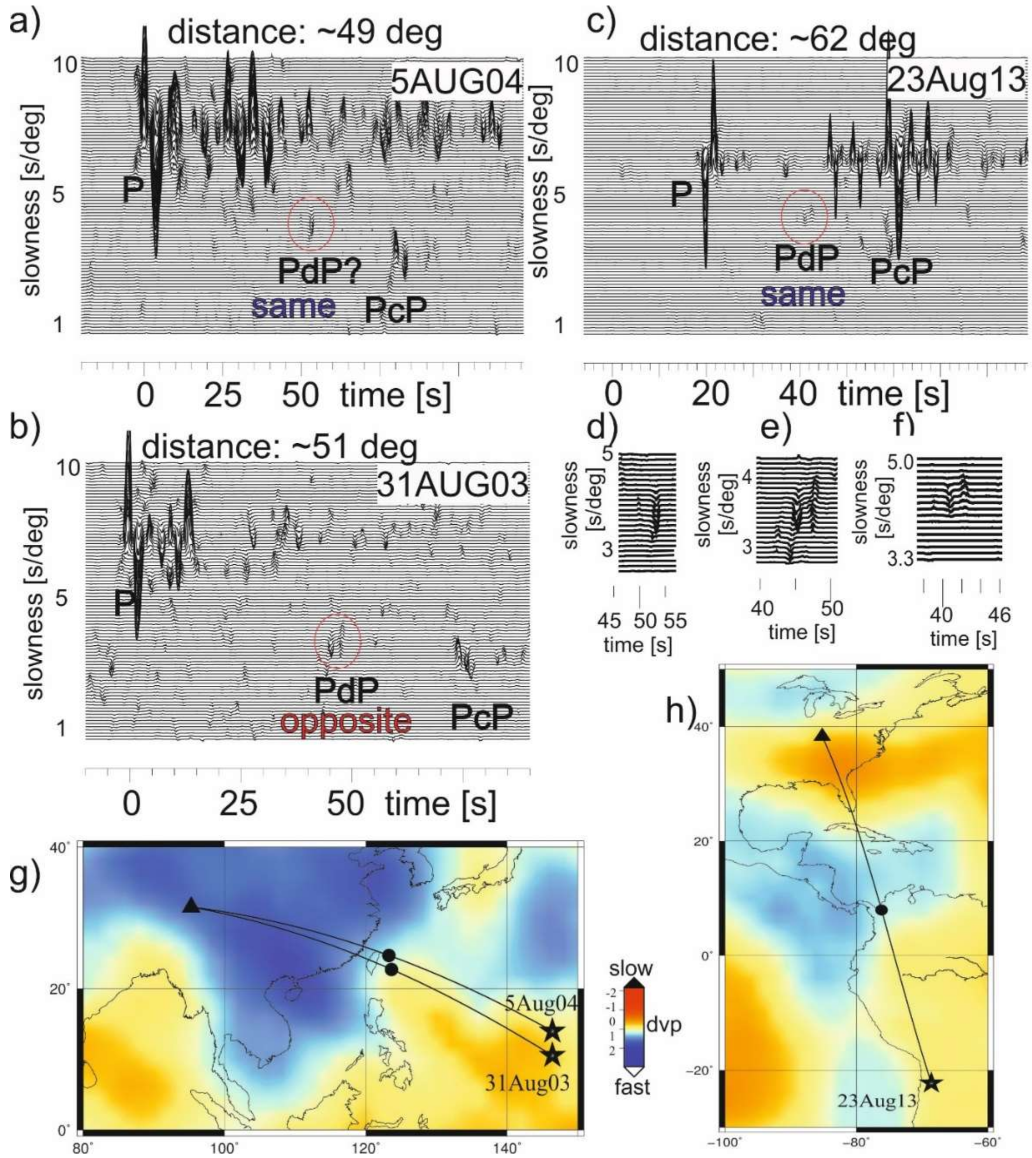

Figure 4: Three examples for 4th root vespagrams showing PdP (circled in red) at short distances. The distance to the central station is given above the vespagrams. a) Event 5-August 2004 recorded at the array in Tibet, b) event 31-August-2003 recorded at the array in Tibet and c) event 23-August 2013 recorded at stations of the TA in Kentucky (Table S2). The polarities are indicated in each vespagram. d), e) and f) show insets around the PdP wave for events in a), b) and c). g) Sources (stars), central station of the array (triangle), great circle path and reflection points (circles) superimposed on a tomographic model MITP08 (Li et al., 2008) for the events in a) and b). h) Same as in g) but for the event in c).

We also re-examined some of the events from Thomas and Laske (2015), who used Ocean Bottom Seismometer (OBS) data of instruments installed around Hawaii, and detected PdP waves at short distances (Tables S1 and S2). These data suffered from noise: however, the polarity of the few events where a D" reflection could be determined, was often the same as PcP and P. Several of the source-receiver combinations were reflected from tomographically fast regions (see Thomas and Laske, 2015) where we might expect the same polarity of PdP compared with P and PcP, but some slow regions were also tested, and the reflections there also showed the same polarity for PdP compared with P and PcP. Figure 5a shows the vespagram for one event where the PdP polarity is clearly visible and is the same as the P and PcP wave. The D" reflection point for this event is in the large low seismic velocity province (LLSVP) as outlined in the P-wave tomography by Li et al. (2008) in Figure 5b. The data for the other two reflection points of the events presented in Thomas and Laske (2015) that reflect nearby (Figure 5b) also show a polarity of PdP matching those of PcP and P.

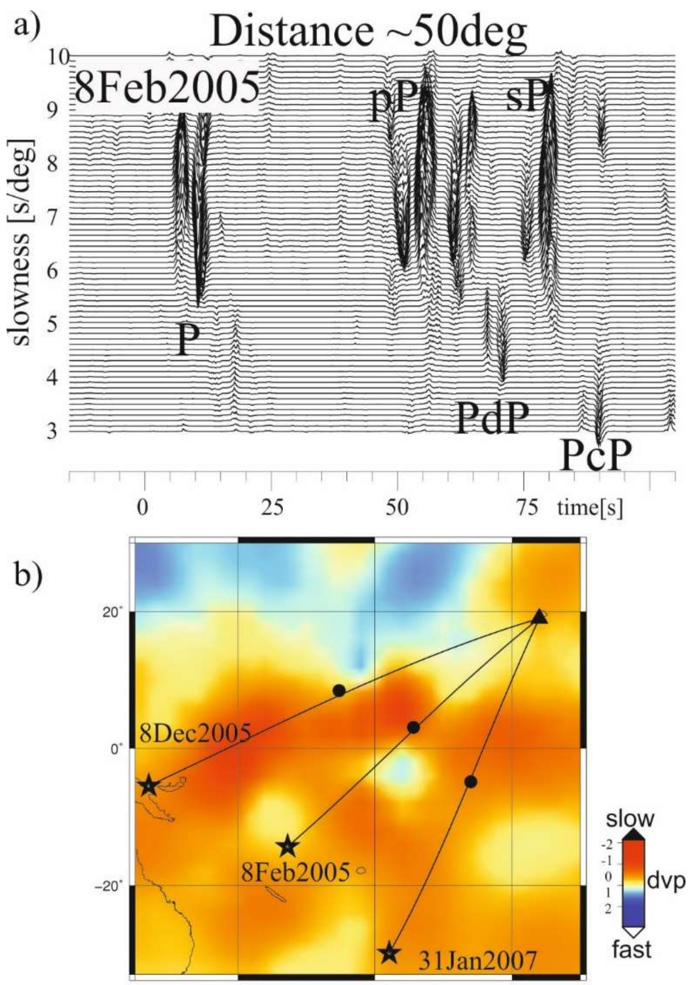

Figure 5: a) As Figure 4a-c) but for event 8-February-2005 recorded at the PLUME array (Table S2). b) As Figure 4f-g) but for the event 8-February-2005. In addition, event locations and reflection points for 8-December-2005 and 31-January-2007 that were analysed and shown in Thomas and Laske (2015) are also indicated.

Taking these new observations into account and looking at published D" reflections, we find that D" reflections for P waves show both positive and negative polarities, not necessarily related to the velocity variations in the mantle mapped by tomography. S-wave reflections from the D" reflector in most regions show the same polarity as the main waves (S and ScS) except for the Pacific (Lay et al., 2006; Ohta et al., 2008). While anisotropy can explain some of this behaviour (e.g., Thomas et al., 2011; Pisconti et al., 2019; 2022), large R-values can also be due to changes in mineralogy. We will explore this scenario here.

4 Thermochemical models and Linear Discriminant Analysis

To understand which parameters are most important in producing large R-values we re-analysed the seismic properties of the thermo-chemical models presented in Cobden and Thomas (2013) and Cobden et al. (2012). The background to the models is explained in Methods 1 in the supplementary material and the parameters are listed in Table 1. We call these models the Mantle simulation. In addition, we also tested models which include a layer of 100 percent MORB below the reflector, where post-perovskite is able to exist (see supplementary material, Table S3). For each simulation, one million unique thermochemical models were produced.

In order to evaluate the R-values, we need to know the velocities and density of each model. First, bulk and shear moduli of the individual minerals were calculated from the elastic parameters published in Stixrude & Lithgow-Bertelloni (2011), using the equation of state in Stixrude & Lithgow-Bertelloni (2005). This involves a 3rd order Birch-Murnaghan equation of state to calculate properties at high pressure, with a Mie Grüneisen correction for thermal pressure (Stixrude and Lithgow-Bertelloni, 2005). All calculations were performed at a pressure of 119 GPa, corresponding to a mantle depth of ~2600 km. The P- and S-wave velocities of both starting (above D") and end (below D") model were then calculated from a Voigt-Reuss-Hill average of the bulk and shear moduli of the individual minerals, and a Voigt average of the density. We pinned the starting model above D" such that the velocities and density fall within 5% of 1D reference model ak135 (Kennett et al., 1995) to avoid extreme outliers. For each model run, we subtract the absolute percentages of the constituent minerals above the reflector from those below it, which yields the changes in composition downward across the boundary. We then evaluated the calculated wave velocities for each model, and performed a detailed analysis of those that produced a ratio of dVs/dVp of 3 and larger across the boundary.

Table1: Ranges of the thermochemical parameters (modelling parameters) as varied between models (Mantle model). See supplementary material (Method 1) for explanation.

Parameter	Minimum value	Maximum value
X. vol% (Mg,Fe)(SiO3 + O)	85	100
Y. vol% (Mg,Fe)SiO3 within X	60	100
Z. vol% FeSi O3 within Y	0	20
K. Fe-Mg part. coeff bm-mw	0.0001	2.0
A. vol% CaSiO3 within (100-X)	0	100
B. vol% SiO2 within (100-X-A)	0	100
P. vol % bm and Al2O3 which converts to ppv	0	100
Temperature (K)	1800	3100

Since one million models is too large a number to consider individually, we turned to Linear Discriminant Analysis (LDA), a powerful statistical technique for classifying existing and new data into predefined discrete groups ("classes"). It is similar to Principal Component Analysis

(PCA) in that it involves data reprojection into an eigenspace with useful properties; in this case: maximising the separability of known classes while taking into account their internal (i.e., class-specific) variance. LDA is different from PCA in that the axes of this eigenspace are non-orthogonal because the eigenvectors are based upon the between-class data scatter scaled by the within-class scatter (Martinez & Kak 2001), rather than the data covariance used in PCA. The technique was first published by Fisher (1936, in Duda & Hart 1973); for a recent treatment, see for example McLachlan (2005). Applying PCA instead would be unsuitable here, as the aim of this study is not to define abstract independent components (comprised of various positive or negative contributions from many inputs), but instead to identify predefined R value-based classes in terms of specific combinations and regimes of the original modelling parameters.

Here, we use LDA as a class "filter" on the full data sets (of modelling and chemical composition parameters, respectively), in order to identify which original model parameters contribute most to class separability, more specifically in distinguishing between low- and high R regimes (i.e., below/above $R = +3$). That is, after LDA reprojection we reject those data that are misclassified in terms of those subsets, thereby reducing the error in the subsequent statistical significance assessment of the input parameters. We also only keep cases for which $R > 1$ (see Method 2 in Supplementary material). The final objective is to construct balanced, distinct profiles of these parameters for low- and high R-values respectively, while distinguishing between two seismological cases: changes in P and S velocity being both positive, or both negative (both of which yield a positive R value). A flow diagram of the process is shown in supplementary Figure S2. The relevant numbers for the datasets and more information on the LDA process are provided in Methods 2 in the supplementary material and in Figure S3.

To simplify subsequent analysis and visualisation of the results, we encoded the two R regimes in the LDA results as variable *Rbool*(ean), with 0 and 1 representing low and high R respectively. Whereas correctly-classified LDA results are discrete, that is, either zero (low-R) or unity (high-R), Rbool is the continuous spatial average of a large number of these points, with equal numbers of low- and high-R cases, when plotted in multidimensional modelling parameter space (Figure 6a, b). Wherever low values dominate (black regions in Figure 6a, b, purple regions in other plots) $R<3$ is predominantly produced, whereas Rbool values close to unity (white regions in Figure 6a, b, orange regions in the other plots) indicate $R>=3$ is dominant.

The Rbool data sets form the basis for the figures in the following section and the supplementary material (Figures 6, 7, S5-S7). To determine which parameters are most relevant for generating large R-values, we also look at the boundary between high and low R-values. If a boundary is vertical, as shown in Figure 6b, mineral C is important for generating large R values while mineral D is not important (likewise for horizontal boundaries, but then mineral C is not important while mineral D is). If the boundary is slanted (Figure 6a) both minerals have to change for generating large R-values. The aim is to thereby identify a) which parameters are most and least relevant for producing $R>=3$, b) which combinations of parameter ranges are necessary and sufficient for this, and c) to what extent transitions between low and high-R regimes are sharp boundaries (steep gradients).

5 Large R-values

Firstly, we look at the case of both P- and S-velocities increasing across the discontinuity for the mantle model (dVp and d$Vs > 0$): our analysis shows that a change from MgSiO3-bridgmanite (bm) to MgSiO3-post-perovskite (ppv) is most important for the generation of R values ≥ 3 (orange-red colours in Figure 6). Figure 6c shows that a decrease of bm is balanced with an increase in ppv for large R-values; however, when comparing the change of MgSiO3 bm to FeSiO3 bm across the boundary, we find that the reduction of MgSiO3 bm is the important parameter, since the dividing line between high and low R-values is almost vertical in Figure 6f. The same is true for MgSiO3-ppv and FeSiO3-ppv in that the MgSiO3-ppv increase is more important that the FeSiO3 increase (Figure S5e).

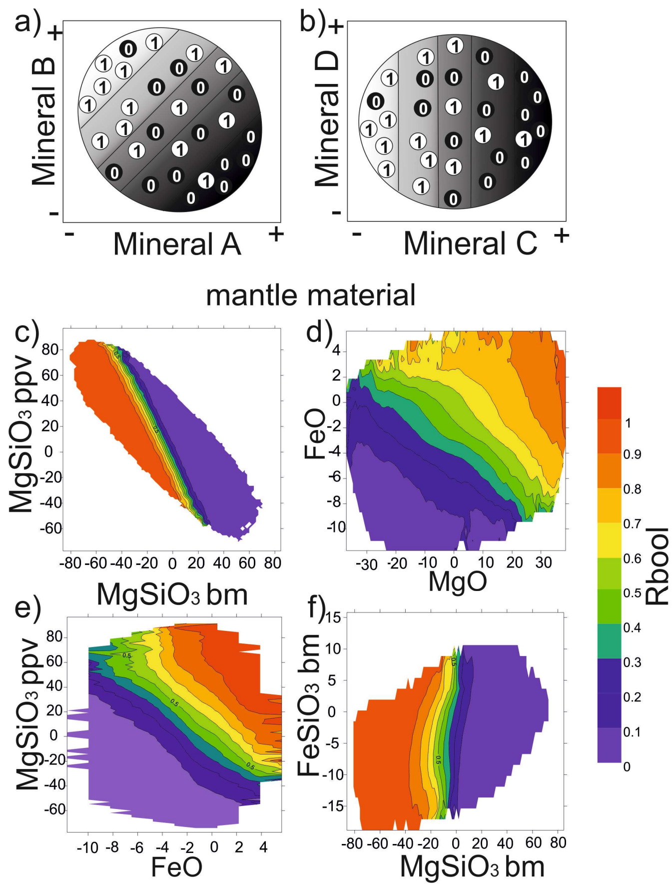

Figure 6: a, b) Explanation for the following plots and the calculation of the local average Rbool, derived from the point cloud of correctly-classified LDA results containing an equal number of low- (0) and high-R cases (1). Black regions mean most values are 0, while in white regions most values are 1. a) For the case that both mineral changes are important for generating large R-values (here decreasing A and increasing B percentages). b) example of mineral C being important for generating large R-values but not mineral D. c) to f) Colour coded Rbool (0, purple: low R-values, i.e., smaller than 3; 1, red: high R-value, i.e., 3 and above) for different combinations of minerals of mantle material (Table 1) as indicated on the diagrams for the case of both Vp and Vs increasing across the D" reflector.

We find that a large increase of MgO across the boundary and a moderate increase of FeO across the boundary can generate large R-values (Figure 6d). But if an increase of FeO is found, then a small increase of Mg-ppv is sufficient for producing large R-values (Figure 6e). Since we find that an increase of MgO can generate R-values ≥ 3, we map MgO, MgSiO3-ppv and MgSiO3-bm and find that the region of high (≥3) and low R-values is separated by a steep and narrow boundary (Figure S6). The figure shows that high R-values are possible for an increase in ppv while bm is decreasing (i.e., a phase transformation) if at the same time MgO is also increasing.

Looking at other parameters (Figure S5), we find that varying temperature does not cause large R-values, since temperature changes seem to induce changes in *Vp* and *Vs* that are comparable in size. Indeed, Deschamps and Trampert (2003) show that temperature variations can lead to an R-value of 1.5 to 2. In our models, the partitioning of iron between bm and ferropericlase also seems to have little influence. Andrault et al. (2010) showed that Fe partitions preferably into bm and leaves post-perovskite Fe-poor. However, we only looked at partitioning between [Mg,Fe]SiO3 and [Mg,Fe]O in our models, and therefore the case described by Andrault et al. (2010) is not represented in our models. Lastly, we find that an increase or decrease of pure SiO2 phase (seifertite), or Al in bridgmanite and/or post-perovskite, do not produce large R-values either.

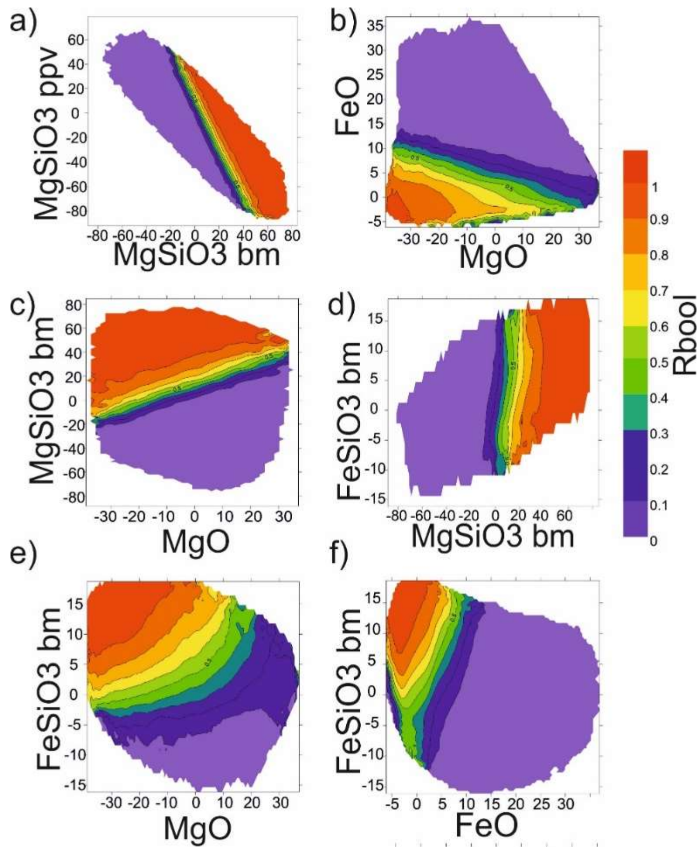

Figure 7: same as Figure 6, but for the case that both Vp and Vs decrease across the D" reflector.

The above-mentioned results were for cases with d*Vp* and d*Vs* > 0. Contrastingly, for d*Vp* and d*Vs* < 0 across the boundary, we find the opposite behaviour: a reduction of FeO and MgO or a decrease of post-perovskite (either FeSiO3-ppv or MgSiO3-ppv) while increasing bm is needed to have large R-values (Figure 7a,b). However, a reduction of ppv across the boundary is unrealistic, since post-perovskite is inferred to be at a depth corresponding to the D" region rather than above it (e.g., Grocholski et al. 2012). This suggests that the most relevant explanation for generating large R-values in regions where the P- and S-velocity are both decreasing is an increase of bm and a reduction of MgO and FeO, with the effect of reducing MgO being stronger than that of reducing FeO.

The dataset of mantle models containing a MORB component (Table S3, Figure S7) shows similar results: For cases where *Vp* and *Vs* both increase across the D" reflector, an increase of ppv and a decrease of bm is the important scenario for producing large R-values. In the case of both velocities decreasing, a reduction of MgO and FeO or a decrease of the amount of ppv with increase of bm across the reflector would generate R-values of 3 and higher. Note that the amount of FeO and MgO come from the non-MORB component in the bulk assemblage, since MORB does not contain MgO or FeO.

6 Discussion

The exact mineralogy of the lowermost mantle is still being debated (e.g., Vilella et al., 2021; Houser et al., 2020; Davies, et al., 2015; Trønnes, 2010; Cobden et al., 2009) and seismological mapping of structures near the core-mantle boundary has helped to test several possibilities of mantle mineralogy. While the mineral phase transition from bridgmanite to post-perovskite seems to be a good explanation for regions of past subduction (e.g. Trønnes, 2010, Hernlund et al., 2005), the mineralogy in the LLSVPs where slower-than-average velocities exit is still not well understood (e.g., Koelemeijer et al., 2021; McNamara, 2019; Deschamps et al., 2012, 2015). In several cases, waves reflecting from layers inside these large low-velocity structures have been used to determine the velocity change across the reflectors (e.g., Lay et al., 2006; Schumacher et al., 2018), which provides a constraint on mineralogy (e.g., Ohta et al., 2008). We use our thermochemical modelling results in combination with PdP and SdS polarity information to constrain mineralogy and causes for the D" reflector.

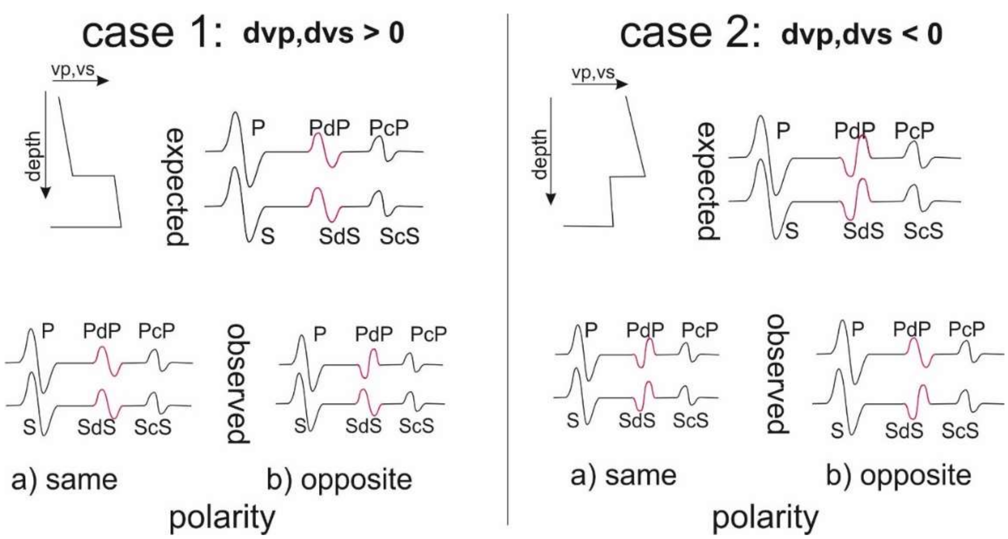

Figure 8: Overview of the different cases: left hand side: Vp and Vs both increasing across the reflector, Case 1, with expected waveforms, right hand side: Vp and Vs both decreasing across the reflector, Case 2, with expected waveforms. The possibilities of observed polarities of PdP (SdS) as (a) same and (b) opposite to P(S) and PcP(ScS) are shown in the bottom row, referring to Cases 1a and 1b and Cases 2a and 2b, respectively, in Table 2.

When interpreting polarity variations in P-and S-waves while ignoring those cases where changes in P-wave and S-wave velocity have opposite signs, there are essentially four possible cases (Figure 8 and Table 2). These four cases separate into two groups where *Vp* and *Vs* both increase (Case 1), and two groups where *Vp* and *Vs* decrease (Case 2), with either the same or opposite polarity of PdP- and SdS-waves.

If *Vp* and *Vs* both increase, and the ratio (R) between S-wave velocity change and P-wave velocity change is between 1 and 3 (Figure 8, case 1a), D" reflection polarities for P- and S-waves are the same as the main phase (P or S) and the CMB reflection. This case been observed in several seismic datasets using P- and S-waves together (e.g. Weber, 1993; Thomas and Weber, 1997; Cobden and Thomas, 2013; Pisconti et al., 2019). Such a scenario could be produced by a thermal anomaly (e.g., Lay et al., 2004; Thomas et al., 2004a), or alternatively, by subducted mid-ocean ridge basalt, MORB (Cobden and Thomas, 2013; Hirose, et al., 1999; Deschamps et al., 2012; Vilella et al., 2021), which is silica-saturated and does not contain ferropericlase. Our modelling shows that an R-value between 1 and 3 can be generated by an increase of bm or a decrease of FeO and MgO (Figure 6, purple colours), and this reduction in bulk (Mg,Fe)O can be indicative of the presence of MORB. Our analyses of mantle models containing a MORB component support this assumption and we therefore conclude that the event shown in Figure 4c is most likely reflections off MORB residing in the D" region, since S-wave observations in this region also show polarities consistent with a velocity increase (Kendall and Nangini, 1996; Lay et al., 2004). For the two events in Figure 4a and b no clear explanation is possible, since we are missing S-wave polarity information for this region.

If, for an S-velocity increase across D", the PdP polarity would indicate a velocity decrease, there are two explanations: Either there is indeed a P-velocity decrease with an associated S-wave velocity increase across the D" reflector, as indicated by e.g., Wookey et al. (2005) for the ppv phase transition in pure MgSiO3. Alternatively, an R-value larger than 3 could generate the same effect (case 1b in Table 2 and Figure 8). Our thermochemical modelling shows that the ppv phase transition is again a good explanation for this scenario (Figure 6, Table 2). Indeed, the contrast of the P-wave velocity across the post-perovskite phase transition has been reported to be between ±1%, while the S-wave change is between 1 and 4% (Oganov and Ono, 2004; Tsuchiya and Tsuchiya, 2006; for an overview see e.g., Cobden et al., 2015).

There is potentially another mechanism that could generate the polarities shown in case 1b: an increase of MgO and FeO across the boundary would also generate large R-values. While the decomposition of (Mg,Fe)-bm into (Mg,Fe)O and SiO2 has been suggested in early experimental studies (e.g., Saxena et al., 1996; Dobrovinsky et al., 1998), more recent studies indicate that the decomposition could have arisen through a problem with the experimental setup (Mao et al., 1997; Gong et al., 2004). Hence, we suggest that the post-perovskite phase transition is the best explanation for observations of PdP polarities opposite those of P and PcP together with SdS polarities the same as S and ScS (case 1b).

Table 2: The four cases shown in Figure 8 with their previous interpretation. In the 3rd row, we provide the R-value associated with the polarities PdP vs SdS in the 1st row and the 4th row explains the mineralogy changes that cause the R-values in row 3. The last row gives our interpretation for each case.

	Case 1a	**Case 1b**	**Case 2a**	**Case 2b**
Polarities, PdP vs. SdS	same	opposite	same	opposite
previous interpretation	MORB, cold slab	ppv (in $MgSiO_3$)	ppv in MORB, seifertite trans.	
R-value range	$1 < R < 3$	$R \geq 3$	$1 < R < 3$	$R \geq 3$
mineralogy change across D"	+bm, -ppv -MgO, -FeO	-bm, +ppv +MgO, +FeO	+ppv, -bm +FeO	+bm, -ppv -MgO, (-FeO)
interpretation with R-value	consistent with MORB	consistent with ppv phase trans.	consistent with ppv phase trans in MORB	primordial material, BEAMs

The mineralogy in low-velocity regions, especially in the LLSVP beneath Africa and the Pacific, is less well constrained, and different mechanisms for velocity discontinuities within LLSVPs have been discussed. Ohta et al. (2008) show that the post-perovskite phase transition in MORB could generate a reflector, but the stishovite to seifertite transition could also be a candidate for this observation (Andrault et al., 2014; Tsuchiya et al. 2004), although the depth of the transition is still debated (Ohta et al., 2008; Grocholski et al., 2013; Sun et al. 2019). Both cases would show polarities of PdP and SdS consistent with a velocity decrease as represented by case 2a in Table 2. Our modelling shows that an R-value below 3 is consistent with the ppv phase transition within MORB while bm decreases.

A velocity decrease for both, P- and S-waves with a ratio of dVs/dVp of ~3 is , on the other hand, indicative of melt in the lower mantle (e.g., Hier-Majumder, 2008; Berryman, 2000), but melt has previously been discussed as cause for ultra-low velocity zones (e.g. Rost et al., 2005, 2006; Yu and Garnero 2019) rather than for a 300 km thick D" layer, and it is still discussed whether melt would stay at the CMB (Thomas et al., 2012; Garnero, 2000). It is difficult to envisage a dynamic mechanism in which thin melt layers would pond 300 km above the CMB, although seismically it would not be incompatible with our observations. A 300 km thick layer of (partial) melt is incompatible with observations of the P and S-wave speed structure within D" (e.g. Cobden et al. 2012).

Lastly, case 2b, where a velocity decrease across the D" reflector is expected in S-waves, but where the PdP polarity suggests a velocity increase (Figure 8, Case 2b), is possibly the rarest observation up to now. We find such a case in the region beneath the western Pacific (Figure 5, see also Thomas and Laske 2015) with PdP waves showing a polarity that is the same as P and PcP in a part of the Pacific LLSVP (Figure 5). Near this region, the S-wave study of Konishi et al. (2009), on the other hand, found a velocity decrease at the top of D" (interpreted there as a phase transition within MORB). While not exactly in the same region, the results by Konishi et al. (2009) together with our results would suggest that our observed P-wave polarity is due to large R-values, and hence would confirm that S-wave velocity reductions are at least 3 times as strong as P-wave velocity reductions in this part of the LLSVP, as also indicated by Koelemeijer et al. (2016, 2018). The reduction of S-wave velocity suggests that MORB itself is not a good explanation for this region (Deschamps et al., 2012), and the P-wave polarity results (Figure 5) indicate that the ppv phase transition is not satisfactory either. Instead, our thermochemical modelling shows that an increase in bm or a decrease in MgO (and to a smaller degree FeO) would generate large R-values.

Ballmer et al. (2016) model the Pacific LLSVP with a combination of MORB and primordial material, which generates a velocity discontinuity at depths consistent with the D" reflector within an LLSVP-like region (Schumacher et al., 2018). Furthermore, Deschamps et al. (2012) and Vilella et al. (2021) show that an increase of bm with an increase of Fe has been suggested to be responsible for the LLSVPs. Their composition is similar to BEAMs (bridgmanite enriched ancient material, Ballmer et al., 2017) and if the BEAMs exists near the CMB (Gülcher et al., 2020) this could explain case 2b in Table 2. Our thermochemical modelling suggests that an increase in bm has the largest effect, but it may also be accompanied with a decrease of FeO (Figure 7f). Interestingly, the studies by Chandler et al. (2021) and Pisconti et al. (2022), although aimed at constraining anisotropy near the edges of an LLSVP, also find that outside the LLSVP ppv is a good explanation, while inside the LLSVP bm explains their observations better.

Our modelling has shown that the different polarity information of P and S-waves, when jointly considered, can aid to constrain the mineralogy of the D" region in different settings. While we are focussing here on isotropic minerals and combinations of minerals above and below the D" reflector to explain polarities, we have to keep in mind that anisotropy is another mechanism that causes polarity changes in seismic waves. For example, Thomas et al. (2011), Pisconti et al. (2019; 2022) and Creasy et al. (2019; 2021) show that polarity variations, especially of P-waves reflected at the D" layer, can also be generated by anisotropy of the D" minerals (ppv, bm, and even ferropericlase), even over small azimuth ranges. The anisotropy, generated by the flow of anisotropic minerals in D", will, however, cause polarity observations that vary with azimuth as shown in Pisconti et al. (2019; 2022); these are unlike the results here, where polarity variations are isotropic. In addition, when anisotropy is present in the D" region, ScS-waves will experience directionally dependent splitting (Nowacki et al. 2011). It has been shown that a combination of splitting measurements together with PdP and SdS polarity observations (Pisconti et al., 2019; 2022), and including discrepant SKS and SKKS splitting measurements (e.g., Creasy et al., 2021) can further constrain mineralogy in the D" region, but the observations vary with azimuth due to the directional velocity variations of the deformed minerals. Therefore, a mapping of regions such as beneath the Caribbean or the western Pacific with crossing paths and taking shear wave splitting of ScS waves into account would help to discriminate between the alternative hypotheses of anisotropy versus large R-values.

7 Conclusion

We have shown that distance-dependent polarity observations of P-wave reflections depend on the ratio of change of S-wave velocity with respect to change in P-wave velocity across the D" reflector, referred to here as the R-value. Linear discriminant analysis (LDA) of mineral composition paired with a set of velocities derived from thermochemical modelling enables us to generate a profile of distinct observable classes (namely, R-values smaller or larger than 3 for regions with velocity increases or decreases), allowing the seismological observables to inform the characterisation of regions in terms of typical mineralogical constituent ratios.

The statistically significant results derived from the thermo-chemical modelling data suggest different causes for large R-values. The post-perovskite phase transition is the best explanation for regions where a velocity increase is detected with S-waves while the P-wave has a polarity that would indicate an apparent velocity decrease. In regions where both D"-reflected P- and S-waves have polarities opposite to the main phases, the ppv phase transition within MORB is likewise the best explanation, as already reported in previous work. A reflection at a MORB layer is consistent with P- and S-wave polarities both suggesting a velocity increase. The last case of an SdS-wave with a polarity opposite to S and ScS but with a PdP-wave suggesting a positive velocity jump across D", as seen in one region of the Pacific LLSVP, can be explained by a reflection off bridgmanite-enriched material, thereby further constraining mineralogy in the LLSVP regions.

Analysing polarities of P- and S-waves, together with extending the epicentral distance range to lower values than previously, and for different regions, thus allows a better classification of the mineralogy change across a reflector. Since variable polarities of P-waves and S-waves can also be generated by anisotropy in the D" region, as shown by Thomas et al. (2011) and Pisconti et al. (2019), a detailed analysis of P- and S-wave observations covering a variety of distances and azimuths is necessary to discriminate between these two hypotheses of large R-values versus anisotropy. Where the former is supported and the latter is absent, inferences can be drawn regarding the most likely mineralogical constituent ratios across the reflector.

Acknowledgements

We would like to thank the Editor, Carolina Lithgow-Bertelloni and two anonymous reviewers for their constructive comments that improved this manuscript. Part of this study was financed by the bilateral ANR-DFG TIMEleSS project (ANR-17-CE31-0025; TH 1530/18-1; SA 2585/3-1; SP1216/8-1), the bilateral PROCOPE-PPP program (PHC 40555PC; DAAD 57390184) and a Vidi grant from the Dutch Research Council (NWO), number 016.Vidi.171.022 (LC). We would like to thank Jennifer Jackson and Carmen Sanchez-Valle for discussions on large R-values and mineralogy in D". Seismic data were analysed with Seismic Handler (Stammler, 1993) and maps were drawn with GMT (Wessels and Smith, 1995). Statistics were performed using the Eigen C++ template library for linear algebra (https://eigen.tuxfamily.org).

Open Research

All data used here are freely accessible through IRIS (Incorporated Research Institutions for Seismology). The dois and references for the datasets are given in the supplementary material Table S2, the events parameters are shown in Table S1.

References

Aki, K and Richards, P. (1980). Quantitative Seismology, vol. I, sec. 5.2.

Andrault, D., Muñoz, M., Bolfan-Casanova, N., Guignot, N., Perrillat, J.P., Aquilanti, G. & Pascarelli, S. (2010). Experimental evidence for perovskite and post-perovskite coexistence throughout the whole D" region. *Earth Planet. Sci. Lett.,* 293, 90–96, Elsevier B.V. doi:10.1016/j.epsl.2010.02.026

Andrault, D., Trønnes, R.G., Konôpková, Z., Morgenroth, W., Liermann, H.P., Morard, G. & Mezouar, M. (2014). Phase diagram and P-V-T equation of state of Al-bearing seifertite at lowermost mantle conditions. *Am. Mineral*., 99, 2035–2042. doi:10.2138/am-2014-4697

Ballmer, M.D.M.D., Schumacher, L., Lekic, V., Thomas, C. & Ito, G. (2016). Compositional layering within the large low shear-wave velocity provinces in the lower mantle. *Geochemistry, Geophys. Geosystems,* 17, 5056–5077. doi:10.1002/2016GC006605

Ballmer, M.D., Houser, C., Hernlund, J.W., Wentzcovitch, R.M. & Hirose, K. (2017). Persistence of strong silica-enriched domains in the Earth's lower mantle. *Nat. Geosci.,* 10, 236–240. doi:10.1038/ngeo2898

Berryman, J.G. (2000). Seismic velocity decrement ratios for regions of partial melt in the lower mantle, *Geophys. Res Lett*. 27, 421-424.

Bortfeld, R., 1961, "Approximations to the reflection and transmission coefficients of plane longitudinal and transverse waves", Geophys. Prosp., 9, 485-502.

Bréger, L & Romanowicz, B, (1998). Three-dimensional structure at the base of the mantle beneath the central Pacific, *Science*, 282, 718–720

Bullen, KE. (1949). Compressibility – pressure hypothesis and the Earth's interior, *Mon. Not. R. Astron. Soc., Geophys. Suppl*. 5 (1949) 355–368

Catalli, K., Shim, S.H. & Prakapenka, V. (2009). Thickness and Clapeyron slope of the post-perovskite boundary. *Nature*, 462, 782–785. doi:10.1038/nature08598

Červený, V. (2001). Seismic ray theory: Cambridge University Press.

Chaloner, J.W., Thomas, C. & Rietbrock, A. (2009). P- and S-wave reflectors in D" beneath southeast Asia. *Geophys. J. Int.,* 179, 1080–1092. doi:10.1111/j.1365-246X.2009.04328.x

Chandler, B.C., Chen, L.-W., Li, M., Romanowicz, B. & Wenk, H.-R. (2021). Seismic anisotropy, dominant slip systems and phase transitions in the lowermost mantle. *Geophys. J. Int.,* 227, 1665–1681, Oxford University Press. doi:10.1093/gji/ggab278

Cobden, L., Goes, S., Ravenna, M., Styles, E., Cammarano, F., Gallagher K. & Connolly J. A. D. (2009). Thermochemical interpretation of 1-D seismic data for the lower mantle: The significance of nonadiabatic thermal gradients and compositional heterogeneity, *J. Geophys. Res.,* 114, B11309, doi:10.1029/2008JB006262

Cobden L., Mosca I., Trampert J. & Ritsema J. (2012). On the likelihood of post-perovskite near the core-mantle boundary: a statistical interpretation of seismic observations. *Phys. Earth Planet. Inter.* 210:21–35

Cobden L. & Thomas C. (2013). The origin of D" reflections: a systematic study of seismic array data sets. *Geophys. J. Int*. 194:1091–1118

Cobden, L., Thomas, C. & Trampert, J. (2015). Seismic detection of post-perovskite inside the Earth. in *Earth's Heterogeneous Mantle*, Springer, 391–440. doi:10.1007/978-3-319-15627-9_13

Cormier V. F. (1982). The effect of attenuation on seismic body waves, *Bull. Seism. Soc. Am.,* 72, S169-S200

Creasy, N., Pisconti, A., Long, M.D., Thomas, C. & Wookey, J. (2019). Constraining lowermost mantle anisotropy with body waves: A synthetic modelling study. *Geophys. J. Int*., 217, 766–783, doi:10.1093/gji/ggz049

Creasy, N., Pisconti, A. Long, M., & Thomas, C., (2021). Modeling of seismic anisotropy observations reveals plausible lowermost mantle flow directions beneath Siberia, *Geochemistry, Geophysics, Geosystems*, 22, e2021GC009924, doi doi.org/10.1029/2021GC009924

Crewes Explorer programs, (2022). Crewes Explorer Programs, accessed July 2022, < https://www.crewes.org/ResearchLinks/ExplorerPrograms>

Davies, D., Kelly, E.J. & Filson, J.R. (1971). Vespa process for analysis of seismic signals, *Nat. Phys. Sci.*, 232, 8–13

Davies, D.R., Goes, S. & Lau, H.C.P. (2015). Thermally dominated deep mantle LLSVP, a review. In *Earth's Heterogeneous Mantle*. Springer, doi:10.1007/978-3-319-15627-9

Deschamps, F., Li, Y. & Tackley, P.J. (2015). Large-Scale Thermo-chemical Structure of the Deep Mantle: Observations and Models. in *Earth's Heterogeneous Mantle*. Springer, doi:10.1007/978-3-319-15627-9

Deschamps, F., Cobden, L. & Tackley, P.J. (2012). The primitive nature of large low shear-wave velocity provinces. *Earth Planet. Sci. Lett.,* 349–350, 198–208. doi:10.1016/j.epsl.2012.07.012

Deschamps, F. & Trampert, J. (2003). Mantle tomography and its relation to temperature and composition. *Phys. Earth Planet. Inter*., 140, 277–291. doi:10.1016/j.pepi.2003.09.004

Dobrosavljevic, V. V., Sturhahn, W. & Jackson, J.M. (2019). Evaluating the role of iron-rich (Mg,Fe)o in ultralow velocity zones. *Minerals*, 9, 1–16. doi:10.3390/min9120762

Dubrovinsky, L., Saxena, S.K. Ahuja, R. & Johansson, B., (1998). Theoretical study of the stability of MgSiO3-perovskite in the deep mantle, *Geophys Res. Lett*., 25, 4253-4256

Duda, R.O. & Hart,P.E. (1973). Pattern Classification and Scene Analysis. *John Wiley & Sons*

Fisher, R.A. (1936). The use of multiple measurements in taxonomic problems, *Annual Eugenics*, 7, Part II, 179-188, doi:10.1111/j.1469-1809.1936.tb02137.x

Frederiksen, A., (2022). Javascript solver for the Zoeppritz equations, Accessed July 2022, < https://home.cc.umanitoba.ca/~frederik/Software/Zoeppritz>

Garnero, E.J. (2000). Heterogeneity of the Lowermost mantle. *Annual Review of Earth and Planetary Sciences*, 28, 509–537, doi.org/10.1146/annurev.earth.28.1.509.

Gong, Z., Fei, Y., Dai, F., Zhang, L. & Jing, F. (2004). Equation of state and phase stability of mantle perovskite up to 140 GPa shock pressure and its geophysical implications *Geophys. Res Lett*., 31, Article Number: L04614

Grocholski, B., Catalli, K., Shim, S.H. & Prakapenka, V. (2012). Mineralogical effects on the detectability of the postperovskite boundary. *Proc. Natl. Acad. Sci. U.S.A.,* 109, 2275–227, doi:10.1073/pnas.1109204109

Grocholski, B., Shim, S.-H. & Prakapenka V. B. (2013). Stability, metastability, and elastic properties ofa dense silica polymorph, seifertite, *J. Geophys. Res.*, 118, 4745–4757, doi:10.1002/jgrb.50360.1

Gülcher, A.J.P., Gebhardt, D.J., Ballmer, M.D. & Tackley, P.J. (2020). Variable dynamic styles of primordial heterogeneity preservation in the Earth's lower mantle. *Earth Planet. Sci. Lett.*, 536, 116160, doi:10.1016/j.epsl.2020.116160

Hernlund, J.W. & Houser, C. (2008). On the statistical distribution of seismic velocities in Earth's deep mantle. *Earth Planet. Sci. Lett*., 265, 423–437. doi:10.1016/j.epsl.2007.10.042

Hernlund, J.W., Thomas, C. & Tackley, P.J. (2005). A doubling of the post-perovskite phase boundary and structure of the Earth's lowermost mantle. *Nature*, 434, 882–886. doi:10.1038/nature03472

Hernlund, J.W. (2010). On the interaction of the geotherm with a post-perovskite phase transition in the deep mantle. *Phys. Earth Planet. Inter*., 180, 222–234, doi:10.1016/j.pepi.2010.02.001

Hier-Majumder, S. (2008). Influence of contiguity on seismic velocities of partially molten aggregates. *J. Geophys. Res. Solid Earth*, **113**, 1–14. doi:10.1029/2008JB005662

Hirose, K., Fei, Y., Ma, Y. & Mao, H.K. (1999). The fate of subducted basaltic crust in the Earth's lower mantle. *Nature*, 397, 53–56. doi:10.1038/16225

Hosseini, K. , Matthews, K. J., Sigloch, K. , Shephard, G. E., Domeier, M. &Tsekhmistrenko, M. (2018). SubMachine: Web-Based tools for exploring seismic tomography and other models of Earth's deep interior. *Geochemistry, Geophysics, Geosystems*, 19. doi:10.1029/2018GC007431

Hosseini, K., Sigloch, K., Tsekhmistrenko, M., Zaheri, A., Nissen-Meyer, T. & Igel, H. (2020). Global mantle structure from multifrequency tomography using P, PP and P-diffracted waves. *Geophys. J. Int*., 220, 96–141. doi:10.1093/gji/ggz394

Houser, C, Hernlund, J.W., Valencia-Cardona, J. & Wentzcovitch, R.M. (2020). Discriminating lower mantle composition, *Phys. Earth Planet. Int.,* 308, 106552, doi.org/10.1016/j.pepi.2020.106552

Hutko, A.R., Lay, T., Revenaugh, J. & Garnero, E.J. (2008). Anticorrelated seismic velocity anomalies from post-perovskite in the lowermost mantle. *Science*, 320, 1070–1074. doi:10.1126/science.1155822

Jackson, J.M. & Thomas, C. (2021). Seismic and Mineral Physics Constraints on the D″ Layer. In *Mantle Convection and Surface Expressions* (eds H. Marquardt, M. Ballmer, S. Cottaar and J. Konter). https://doi.org/10.1002/9781119528609.ch8

Karato, S.-I. & Karki, B.B. (2001). Origin of lateral variation of seismic wave velocity and density in the deep mantle. *J. Geophys. Res.,* 106, 21771–21783

Kawai, K. & Geller, R.J. (2010). Waveform inversion for localized seismic structure and an application to D″ structure beneath the Pacific. *J. Geophys. Res.,* 115, 1–15. doi:10.1029/2009jb006503

Kendall, J-M.& Nangini, C. (1996). Lateral variations in below the Caribbean, *Geophys. Res. Lett*., 23, 399–402

Kennett B., Engdahl E., Buland R. (1995). Constraints on seismic velocities in the Earth fromtravel-times. *Geophys J Int* 122:108–124

Kito, T., Rost, S., Thomas, C. & Garnero, E.J. (2007). New insights into the P- and S-wave velocity structure of the D″ discontinuity beneath the Cocos plate. *Geophys. J. Int.,* 169, 631–645. doi:10.1111/j.1365-246X.2007.03350.x

Koelemeijer, P., Ritsema, J., Deuss, A. & van Heijst, H.J. (2016). SP12RTS: A degree-12 model of shear- and compressional-wave velocity for Earth's mantle. *Geophys. J. Int.,* 204, 1024–1039. doi:10.1093/gji/ggv481

Koelemeijer, P., Schuberth, B.S.A., Davies, D.R., Deuss, A. & Ritsema, J. (2018). Constraints on the presence of post-perovskite in Earth's lowermost mantle from tomographic-geodynamic model comparisons. *Earth Planet. Sci. Lett.,* 494, 226–238. doi:10.1016/j.epsl.2018.04.056

Koelemeijer, P. (2021). Toward Consistent Seismological Models of the Core–Mantle Boundary Landscape. *In Mantle Convection and Surface Expressions* (eds H. Marquardt, M. Ballmer, S. Cottaar and J. Konter). https://doi.org/10.1002/9781119528609.ch9

Konishi, K., Kawai, K., Geller, R.J. & Fuji, N. (2009). MORB in the lowermost mantle beneath the western Pacific: Evidence from waveform inversion. *Earth Planet. Sci. Lett.,* 278, 219–225, Elsevier B.V. doi:10.1016/j.epsl.2008.12.002

Kuwayama, Y., Hirose, K., Cobden, L., Kusakabe, M., Tateno, S., & Ohishi, Y. (2022). Post-perovskite phase transition in the pyrolitic lowermost mantle: Implications for ubiquitous occurrence of post-perovskite above CMB. Geophys. Res. Lett., 49, e2021GL096219. doi.org/10.1029/2021GL096219

Lay, T. (2008). Sharpness of the D″ discontinuity beneath the Cocos plate: Implications for the perovskite to post-perovskite phase transition. *Geophys. Res. Lett*., 35, 1–5. doi:10.1029/2007GL032465

Lay, T. (2015). Deep Earth Structure: Lower Mantle and D". *Treatise Geophys*. Second Ed., Vol. 1, Elsevier B.V. doi:10.1016/B978-0-444-53802-4.00019-1

Lay, T. & Helmberger D.V. (1981). Body wave amplitude patterns and upper mantle attenuation variations across North America, *Geophys. J.* 68, 691-726

Lay T & Helmberger D.V. (1983). A lower mantle S-wave triplication and the shear velocity structure of D″. *Geophys J Roy Astron Soc*., 75:799–837

Lay, T., Garnero, E.J. & Russell, S.A. (2004). Lateral variation of the D″ discontinuity beneath the Cocos Plate. *Geophys. Res. Lett.,* 31. doi:10.1029/2004GL020300

Lay, T. & Garnero, E.J. (2004). Core-Mantle Boundary Structures and Processes. In *The State of the Planet: Frontiers and Challenges in Geophysics* (eds R. Sparks and C. Hawkesworth). doi: 10.1029/150GM04

Lay T., Hernlund J., Garnero E.J. & Thorne MS (2006) A post-perovskite lens and D″ heat flux beneath the central Pacific. *Science* 314:1272–1276

Li, C., Hilst, R.D. Van Der, Engdahl, E.R. & Burdick, S. (2008). A new global model for P wave speed variations in Earth's mantle. *Geochemistry, Geophys. Geosystems,* 9. doi:10.1029/2007GC001806

Malcolm, A.E. & Trampert, J. (2011) Tomographic errors from wave front healing: More than just a fast bias. *Geophys. J. Int.*, **185**, 385–402. doi:10.1111/j.1365-246X.2011.04945.x

Martinez, A. M. & Kak, A. C. (2001). PCA versus LDA. *IEEE Transactions on Pattern Analysis and Machine Intelligence*. 23, 228–233. doi:10.1109/34.908974

Masters G., Laske G., Bolton H. & Dziewonski A.M. (2000). The relative behaviour of shear velocity, bulk sound speed, and compressional velocity in the mantle: implications for chemical and thermal structure. In: Karato S, Forte A, Liebermann R, Masters G, Stixrude L (eds) *Earth's deep interior: mineral physics and tomography from the atomic to the global scale*, vol 117. AGU, Washington D.C., pp 63–87

Mao, H. K., Shen G. & Hemley, R. J. (1997). Multivariable Dependence of Fe-Mg Partitioning in the Lower Mantle. *Science* 278, 2098

McLachlan, G. J. (2005). *Discriminant Analysis and Statistical Pattern Recognition*. Vol. 583, John Wiley & Sons

McNamara, A.K. (2019). A review of large low shear velocity provinces and ultra low velocity zones. *Tectonophysics,* 760, 199–220, doi:10.1016/j.tecto.2018.04.015

Moore, M.M., Garnero, E.J., Lay, T. & Williams, Q. (2004). Shear wave splitting and waveform complexity for lowermost mantle structures with low-velocity lamellae and transverse isotropy. *J. Geophys. Res. Solid Earth*, 109, 1–26. doi:10.1029/2003jb002546

Müller, G., (1985). The reflectivity method: a tutorial, *J. Geophys.,* 58, 153–174

Müller, G. (2007): Theory of elastic waves, (Scientific Technical Report STR ; 07/03), Potsdam : Deutsches GeoForschungsZentrum GFZ, 228 p. https://doi.org/10.2312/GFZ.b103-07037

Muirhead, K.J. & Datt, R., (1976). The N-th root process applied to seismic array data, *Geophys, J. R.* astr. Soc., 47, 197–210

Murakami M., Hirose K., Kawamura K., Sata N. & Ohishi Y. (2004). Post-perovskite phase transition in MgSiO3. *Science* 304:855–858

Oganov A.R. & Ono S. (2004). Theoretical and experimental evidence for a post-perovskite phase ofMgSiO3 in Earth's D″ layer. *Nature* 430:445–448

Ohta, K., Hirose, K., Lay, T., Sata, N. & Ohishi, Y. (2008). Phase transitions in pyrolite and MORB at lowermost mantle conditions: Implications for a MORB-rich pile above the core-mantle boundary. *Earth Planet. Sci. Lett.,* 267, 107–117. doi:10.1016/j.epsl.2007.11.037

Pisconti, A., Thomas, C. & Wookey, J. (2019). Discriminating between causes of D″ anisotropy using reflections and splitting measurements for a single path. *J. Geophys. Res. Solid Earth*, 124, 4811–4830. doi:10.1029/2018JB016993

Pisconti, A, Creasy, N., Wookey, J., Long, M. & Thomas, C. (2022). Mineralogy, fabric, and deformation domains in D" across the southwestern border of the African LLSVP, in review, *Geophys. J. Int.*

Ritsema, J., Deuss, A., Heijst, H.J. Van & Woodhouse, J.H. (2011). S40RTS: A degree-40 shear-velocity model for the mantle from new Rayleigh wave dispersion, teleseismic traveltime and normal-mode splitting function measurements. *Geophys. J. Int*., 184, 1223–1236. doi:10.1111/j.1365-246X.2010.04884.x

Rochira, F. & Thomas, C. (2022). Mapping the edge of subducted slabs in the lower mantle beneath India, Geophys. J. Int. 230, 1239-1252, doi.org/10.1093/gji/ggac110

Romanowicz, B. & Wenk, H.R. (2017) Anisotropy in the deep Earth. *Phys. Earth Planet. Inter.*, **269**, 58–90. doi:10.1016/j.pepi.2017.05.005

Rost, S. & Thomas, C., (2002). Array seismology: methods and applications, *Rev. Geophys.,* 40, doi:10.1029/2000RG000100

Rost, S., Garnero, E.J., Williams, Q. & Manga, M. (2005). Seismological constraints on a possible plume root at the core-mantle boundary. *Nature*, 435, 666–669. doi:10.1038/nature03620

Rost, S., E. J. Garnero, and Q. Williams (2006), Fine-scale ultralow-velocity zone structure from high-frequency seismic array data, J. Geophys. Res., 111, B09310, doi:10.1029/2005JB004088.

Saxena, S. K., Dubrovinsky, L. S., Lazor, P., Cerenius, Y., Haggkvist, P., Hanfland, M. & Hu, J., (1996). Stability of perovskite (MgSiO3) in the Earth's mantle, *Science*, 274,1357-1359

Scherbaum, F., Krüger, F., & Weber, M. (1997). Double beam imaging: mapping lower mantle heterogeneities using combinations of source and receiver arrays. *J Geophys Res Solid Earth*,102, 507–522

Schimmel, M. & Paulssen, H. (1996). Steeply reflected ScSH precursors from the D" region. *J. Geophys. Res. Solid Earth*, 101, 16077–16087. doi:10.1029/96jb00934

Schumacher, L. & Thomas C. (2016). Detecting lower mantle slabs beneath Asia and the Aleutians, Geophys. J. Int., 205, 1512-1524

Schumacher, L., Thomas, C. & Abreu, R. (2018). Out-of-plane seismic reflections beneath the Pacific and their geophysical implications. *J. Geophys. Res. Solid Earth*, 123, 2286–2302. doi:10.1002/2017JB014728

Schweitzer, J., Fyen, J., Mykkeltveit, S. & Kvaerna, T. (2002). Seismic Arrays. *In New Manual of Seismological Observatory Practice*-NMSOP, IASPEI, pp. 481–532

Shim, S.H. (2008). The postperovskite transition. *Annu. Rev. Earth Planet. Sci.,* 36, 569–599. doi:10.1146/annurev.earth.36.031207.124309

Shim, S.H., Duffy, T.S., Jeanloz, R. & Shen, G. (2004). Stability and crystal structure of MgSiO3 perovskite to the core-mantle boundary. *Geophys Res Lett.,* 31, L10603

Simmons, N.A., Forte, A.M., Boschi, L. & Grand, S.P. (2010). GyPSuM: A joint tomographic model of mantle density and seismic wave speeds. *J. Geophys. Res. Solid Earth*, 115, 1–24. doi:10.1029/2010JB007631

Sollberger, D., Greenhalgh, S.A., Schmelzbach, C., Renterghem, C. Van & Robertsson, J.O.A. (2018) 6-C polarization analysis using point measurements of translational and rotational ground-motion: Theory and applications. *Geophys. J. Int.*, **213**, 77–97. doi:10.1093/gji/ggx542

Stammler, K. (1993). Seismichandler Programmable Multichannel Data Handler for Interactive and Automatic Processing of Seismological Analyses, *Comput.Geosci.*, 19, 135-140

Stixrude, L. & Lithgow-Bertelloni, C. (2005) Thermodynamics of mantle minerals—I. Physical properties. *Geophys J. Int*., 162, 610–632

Stixrude, L. & Lithgow-Bertelloni, C. (2011). Thermodynamics of mantle minerals - II. Phase equilibria. *Geophys. J. Int.,* 184, 1180–1213. doi:10.1111/j.1365-246X.2010.04890.x

Sun, N., Shi, W., Mao, Z., Zhou, C. & Prakapenka, V.B. (2019). High Pressure-Temperature Study on the Thermal Equations of State of Seifertite andCaCl2-Type SiO2. *J. Geophys. Res. Solid Earth*, 124, 12620–12630. doi:10.1029/2019JB017853

Tatham R.H. & Krail, P.M. (2012), "Zero crossings, the elastic Brewster's angle and physical insight into shear-wave reflections," *SEG Technical Program Expanded Abstracts* : 1-5. https://doi.org/10.1190/segam2012-1286.1

Thomas, C. & Laske, G. (2015). D″ observations in the Pacific from PLUME ocean bottom seismometer recordings. *Geophys. J. Int*., 200, 851–862. doi:10.1093/gji/ggu441

Thomas, C. & Weber, M. (1997). P velocity heterogeneities in the lower mantle determined with the German Regional Seismic Network: Improvement of previous models and results of 2D modelling. *Phys. Earth Planet. Inter.*, 101, 105–117. doi:10.1016/S0031-9201(96)03245-1

Thomas, Ca. Weber, M.Agnon, A. & Hofstetter, A. (1998). A low velocity lamella in D", *Geophys. Res. Lett*., 25, 2885-2888

Thomas, C., Kendall, J.M. & Lowman, J. (2004a). Lower-mantle seismic discontinuities and the thermal morphology of subducted slabs. *Earth Planet. Sci. Lett*., 225, 105–113. doi:10.1016/j.epsl.2004.05.038

Thomas, C., Garnero, E.J. & Lay, T. (2004b). High-resolution imaging of lowermost mantle structure under the Cocos plate. *J. Geophys. Res. Solid Earth*, 109, 834–835. doi:10.1029/2004JB003013

Thomas, C., Wookey, J., Brodholt, J. & Fieseler, T. (2011) Anisotropy as cause for polarity reversals of D″ reflections. *Earth Planet Sci Lett*. 307, 369–376

Thomas, C.W., Liu, Q., Agee, C.B., Asimow, P.D. & Lange, R.A. (2012) Multi-technique equation of state for Fe2SiO4 melt and the density of Fe-bearing silicate melts from 0 to 161 GPa. *J. Geophys. Res. Solid Earth*, **117**, 1–19. doi:10.1029/2012JB009403

Thorne, M.S., Lay, T., Garnero, E.J., Jahnke, G. & Igel, H. (2007). Seismic imaging of the laterally varying D″ region beneath the cocos plate. *Geophys. J. Int.,* 170, 635–648. doi:10.1111/j.1365-246X.2006.03279.x

Trønnes, R.G. (2010). Structure, mineralogy and dynamics of the lowermost mantle. *Mineral. Petrol*., 99, 243–261. doi:10.1007/s00710-009-0068-z

Tsuchiya, T. & Tsuchiya, J. (2006). Effect of impurity on the elasticity of perovskite and postperovskite: velocity contrast across the postperovskite transition in (Mg, Fe, Al)(Si, Al)O3. *Geophys Res Lett*, 33, L12S04

Tsuchiya, T., Tsuchiya, J., Umemoto, K. & Wentzcovitch, R. (2004) Phase transition in MgSiO3 perovskite in the Earth's lower mantle. *Earth Planet Sci Lett.,* 224, 241–248

Vilella, K., Bodin, T., Boukaré, C.E., Deschamps, F., Badro, J., Ballmer, M.D. & Li, Y. (2021). Constraints on the composition and temperature of LLSVPs from seismic properties of lower mantle minerals. *Earth Planet. Sci. Lett.,* 554. doi:10.1016/j.epsl.2020.116685

Weber, M. (1993). P-wave and S-wave reflections from anomalies in the lowermost mantle. *Geophys J Int.,* 115, 183–210

Wentzcovitch, R.M., Tsuchiya, T. & Tsuchiya, J. (2006). MgSiO(3) postperovskite at D″ conditions. *Proc Natl Acad Sci USA,* 103, 543–546

Wessel, P. & Smith, W.H.F. (1995). New version of the Generic Mapping Tools released, *EOS Transact. Amer. Geophys.Union*, 76, 329

Williams, Q. & Garnero, E.J. (1996). Seismic Evidence for Partial Melt at the Base of Earth's Mantle. *Science*, 273, 1528–1530, doi:10.1126/science.273.5281.1528

Wookey, J., Stackhouse, S.,Kendall, J.M., Brodholt, J.P.& Price, G.D., (2005). Efficacy of the post-perovskite phase as an explanation of lowermost mantle seismic properties, *Nature*, 438, 1004–1008

Wysession, M.E., Lay, T., Revenaugh, J., Williams, Q., Garnero, E.J., Jeanloz, R. & Kellogg, L.H. (1998). The D" discontinuity and its implications, in *The Core-Mantle Boundary Region*, Geodyn. Ser., vol. 28, edited by M. Gurnis et al., AGU, Washington D. C., pp. 273– 297

Yang, K., Dong, X. & Zhang, J. (2021) Polarity-reversal correction for vector-based elastic reverse time migration. *Geophysics*, **86**, S45–S58. doi:10.1190/geo2020-0033.1

Young, C.J. & Lay, T. (1990) Multiple phase-analysis of the shear velocity structure in the D" region beneath Alaska. *J Geophys Res Solid Earth Planets* 95, doi: 10.1029/90JB01081

Yu, S. & Garnero, E.J. (2018) .Ultralow Velocity Zone Locations: A Global Assessment. *Geochemistry, Geophys. Geosystems*, **19**, 396–414. doi:10.1002/2017GC007281

Zoeppritz, K. (1919). Über Reflexion und Durchgang seismischer Wellen durch Unstetigkeitsflächen. *Göttinger Nachr.,* 66-84